AGU PUBLICATIONS

Global Biogeochemical Cycles

RESEARCH ARTICLE

10.1002/2016GB005406

Key Points:
- Atmospheric methane is growing rapidly
- Isotopic evidence implies that the growth is driven by biogenic sources
- Growth is dominated by tropical sources

Supporting Information:
- Supporting Information S1

Correspondence to:
E. G. Nisbet,
e.nisbet@rhul.ac.uk

Citation:
Nisbet, E. G., et al. (2016), Rising atmospheric methane: 2007–2014 growth and isotopic shift, *Global Biogeochem. Cycles*, *30*, doi:10.1002/2016GB005406.

Received 3 MAR 2016
Accepted 2 SEP 2016
Accepted article online 26 SEP 2016

Rising atmospheric methane: 2007–2014 growth and isotopic shift

E. G. Nisbet[1], E. J. Dlugokencky[2], M. R. Manning[3], D. Lowry[1], R. E. Fisher[1], J. L. France[1,4], S. E. Michel[5], J. B. Miller[5,6], J. W. C. White[5], B. Vaughn[5], P. Bousquet[7], J. A. Pyle[8,9], N. J. Warwick[8,9], M. Cain[8,9], R. Brownlow[1], G. Zazzeri[1], M. Lanoisellé[1], A. C. Manning[4], E. Gloor[10], D. E. J. Worthy[11], E.-G. Brunke[12], C. Labuschagne[12,13], E. W. Wolff[14], and A. L. Ganesan[15]

[1]Department of Earth Sciences, Royal Holloway, University of London, Egham, UK, [2]US National Oceanic and Atmospheric Administration, Earth System Research Laboratory, Boulder, Colorado, USA, [3]Climate Change Research Institute, School of Geography Environment and Earth Sciences, Victoria University of Wellington, Wellington, New Zealand, [4]Centre for Ocean and Atmospheric Sciences, School of Environmental Sciences, University of East Anglia, Norwich, UK, [5]Institute of Arctic and Alpine Research, University of Colorado Boulder, Boulder, Colorado, USA, [6]Cooperative Institute for Research in Environmental Sciences, University of Colorado Boulder, Boulder, Colorado, USA, [7]Laboratoire des Sciences du Climat et de l'Environnement, Gif-sur-Yvette, France, [8]Department of Chemistry, University of Cambridge, Cambridge, UK, [9]National Centre for Atmospheric Science, Cambridge, UK, [10]School of Geography, University of Leeds, Leeds, UK, [11]Environment Canada, Downsview, Ontario, Canada, [12]South African Weather Service, Stellenbosch, South Africa, [13]School of Physical and Chemical Sciences, North-West University, Potchefstroom, South Africa, [14]Department of Earth Sciences, University of Cambridge, Cambridge, UK, [15]School of Geographical Sciences, University of Bristol, Bristol, UK

Abstract From 2007 to 2013, the globally averaged mole fraction of methane in the atmosphere increased by 5.7 ± 1.2 ppb yr^{-1}. Simultaneously, $\delta^{13}C_{CH4}$ (a measure of the $^{13}C/^{12}C$ isotope ratio in methane) has shifted to significantly more negative values since 2007. Growth was extreme in 2014, at 12.5 ± 0.4 ppb, with a further shift to more negative values being observed at most latitudes. The isotopic evidence presented here suggests that the methane rise was dominated by significant increases in biogenic methane emissions, particularly in the tropics, for example, from expansion of tropical wetlands in years with strongly positive rainfall anomalies or emissions from increased agricultural sources such as ruminants and rice paddies. Changes in the removal rate of methane by the OH radical have not been seen in other tracers of atmospheric chemistry and do not appear to explain short-term variations in methane. Fossil fuel emissions may also have grown, but the sustained shift to more ^{13}C-depleted values and its significant interannual variability, and the tropical and Southern Hemisphere loci of post-2007 growth, both indicate that fossil fuel emissions have not been the dominant factor driving the increase. A major cause of increased tropical wetland and tropical agricultural methane emissions, the likely major contributors to growth, may be their responses to meteorological change.

1. Introduction

The methane content of the atmosphere began rising again in 2007 after a growth slowdown that had first become apparent in the late 1990s [*Dlugokencky et al.*, 1998; *Nisbet et al.*, 2014]. The mole fraction of Southern Hemisphere atmospheric methane varied little for 7 years up to 2006 but then started to increase in early 2007. Since 2007, sustained increases in atmospheric methane mole fraction have occurred in most latitudinal zones of the planet but with major local short-term excursions from the overall spatial pattern of growth (Figure 1). In the Northern Hemisphere autumn of 2007, rapid growth was measured in the Arctic and boreal zone (Figure 1). However, both in 2007 and thereafter, global growth has dominantly been driven by the latitudes south of the Arctic/boreal zone, for example, both north and south of the equator in 2008 and in the southern tropics in 2010–2011. Even compared to the increases of preceding years, 2014 was exceptional, with extremely strong annual (1 January 2014 to 1 January 2015) growth at all latitudes, especially in the equatorial belt (Figure 1).

CH_4 mole fractions provide insufficient information to determine definitively the causes of the recent rise [*Kirschke et al.*, 2013]. Isotopic measurements [*Dlugokencky et al.*, 2011] provide powerful constraints that can help to identify specific source contributions. Atmospheric methane is also becoming more depleted in the isotope ^{13}C. At any individual location, local meteorological factors such as shifting prevailing wind directions may influence measurements: however, the sustained nature of the increase and isotopic shift, and the regional and global distribution of the methane growth, implies that major ongoing changes in methane budgets are occurring.

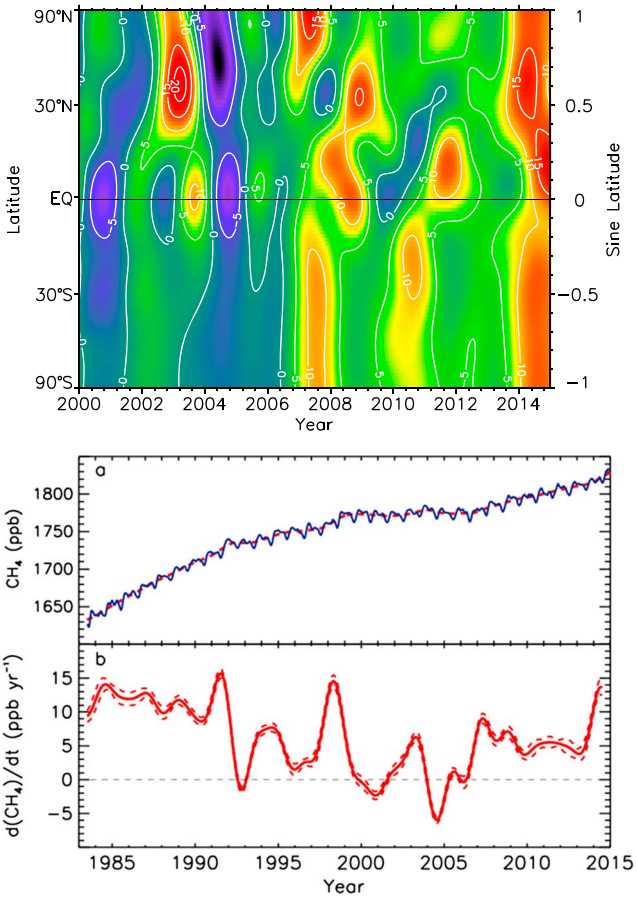

Figure 1. Global trends in CH_4 from 2000 to the end of 2014. (top) Global sine latitude versus time plot of CH_4 growth rate. Green, yellow, and red colors show increases; blue, dark blue, and violet show declines, contoured in increments of 5 ppb yr^{-1}. (bottom) Globally averaged methane and growth rates in 1983–2014. Plot a shows atmospheric mole fraction. Red dashed line is a deseasonalized trend curve fitted to the global averages. Plot b shows instantaneous growth rate from the time derivative of the red dashed line in plot a. Thin dashed lines are ±1 standard deviation.

Recently, *Schaefer et al.* [2016] used a one-box model of CH_4 mole fraction and $\delta^{13}C_{CH4}$ isotopic data to reconstruct the global history of CH_4 emissions to the atmosphere. They concluded that the isotopic evidence demonstrates that emissions of thermogenic methane (e.g., from fossil fuels and biomass burning) were not the dominant cause of the post-2007 growth and pointed out that this contradicts emission inventories. In contrast, *Schaefer et al.* [2016] concluded that the cause of the post-2007 rise was primarily an increase in biogenic emissions and that these emissions were located outside the Arctic. Furthermore, they inferred that the increased emissions were probably more from agricultural sources than from wetlands.

The evidence reported here includes new Atlantic and Arctic methane mole fraction and isotopic data and develops the analysis by using a running budget analysis (see supporting information S1, section 16) of monthly averages over four latitude zones instead of annual averages and a one-box model. This detailed analysis permits latitudinal differentiation of changes in CH_4 emission sources, which our isotopic data show have significant interannual variability in the overall trend to more negative values since 2007.

Figure 1 illustrates the CH_4 record over the three decades since the start of detailed global monitoring by NOAA (http://www.esrl.noaa.gov/gmd/ccgg/trends_ch4/). The very high growth rates in the 1980s (~14 ppb in 1984 and $>$10 ppb yr^{-1} through 1983–1991) [*Dlugokencky et al.*, 1998; *Dlugokencky et al.*, 2011] were driven by the strong increase in anthropogenic emissions in the post-War years, for example, from the Soviet gas industry [*Dlugokencky et al.*, 1998]. In 1992 the eruption of Mt. Pinatubo and the major El Niño event had important impacts on sources and sinks. Following this, growth rates declined. Major reductions in leaks from the gas industry may have contributed to the reduction in growth rates [*Dlugokencky et al.*, 1998]. Strong growth resumed briefly during the strong El Niño event of 1997–1998, but apart from this single event, methane growth rates were subdued in the period 1992–2007. The overall trend from 1983 to 2007 is consistent with an approach to equilibrium [*Dlugokencky et al.*, 2011], implying no trend in total global emissions and an atmospheric lifetime of approximately 9 years.

2. Methods

Observations reported here are from measurements made by the USA National Oceanic and Atmospheric Administration (NOAA) Cooperative Global Air Sampling Network, for whom the Institute of Arctic and Alpine Research (INSTAAR) carry out $\delta^{13}C_{CH4}$ measurement on a subset of the same air samples analyzed for CH_4, by Royal Holloway, University of London (RHUL, UK), and by the University of Heidelberg (UHEI). Details are

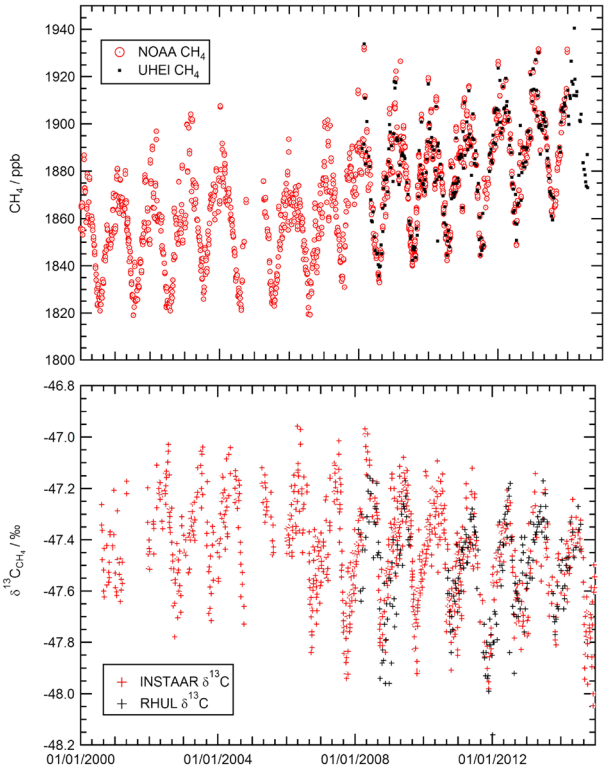

Figure 2. (top) Methane mole fraction and (bottom) $\delta^{13}C_{CH4}$ isotope measurements in discrete air samples collected from Alert, Canada. Mole fraction data from NOAA and University of Heidelberg (UHEI) samples; isotopic measurements from NOAA-INSTAAR and RHUL.

given in the supporting information S1, sections 6–8. Mole fraction measurements are reported on the World Meteorological Organization X2004A scale [*Dlugokencky et al.*, 2005 updated at http://www.esrl.noaa.gov/gmd/ccl/ch4_scale.html].

By comparing data from different laboratories, we have checked for systematic bias among the measurement programs. Further details on RHUL-INSTAAR intercomparison are in the supporting information S1, sections 8–10.

3. Measurements

To understand the factors driving global methane trends in the past decade, we focus on key background stations in regions where significant methane events have occurred: (1) the Arctic and boreal zone, (2) the Atlantic equatorial tropics, and (3) the Southern Hemisphere.

From 2007 to 2013, we report that the globally averaged mole fraction of methane in the atmosphere increased by 5.7 ± 1.2 ppb yr^{-1} (parts per billion, or nmole mol^{-1}, dry air, ±1 standard deviation of annual increases; uncertainty of each annual increase is ~ ±0.5 ppb yr^{-1}). Growth has continued strongly with an increase of 12.5 ± 0.4 ppb in 2014. Simultaneously, results presented here show that $\delta^{13}C_{CH4}$ (a measure of the $^{13}C/^{12}C$ isotope ratio in methane) has recently shifted significantly to more negative values. For example, prior to 2007, as monitored in remote equatorial Southern Hemisphere air at Ascension Island, $\delta^{13}C_{CH4}$ was stable or increased slightly, with $\delta^{13}C_{CH4}$ changing by less than +0.01‰ yr^{-1}. Post 2007, $\delta^{13}C_{CH4}$ started to decrease. The shift has been in excess of −0.03‰ yr^{-1}, with a total shift of -0.24 ± 0.02‰ by 2014. Similar patterns to those observed at Ascension have been observed globally, though with regional variation (Figure S10).

3.1. Methane $\delta^{13}C_{CH4}$ in High Northern Latitudes: Alert, Canada (82°27′N, 62°31′W)

Methane mole fractions (Figure 2, top and Figure S1) in NOAA air samples from Alert, Nunavut, Canada, which are representative of the western Arctic, show a sharp increase in summer 2007. In September 2007, methane measured at Alert was 16 ppb higher than in the previous September, although note that single-month comparisons can depend heavily on sustained local meteorological conditions. That year, the annual increase averaged over 53°N to 90°N was 13.3 ± 1.3 ppb. But this was not sustained. In 2008, 2010, and markedly so in 2011–2012, Arctic growth was below global means. As fast horizontal mixing at high latitudes efficiently links Arctic emission zones with Alert [*Bousquet et al.*, 2011], this indicates that from 2008 to 2013 no major sustained new methane emission increase occurred in the wider Arctic. In 2014, year-on-year strong Arctic increases began anew (Figure S1) but at a rate comparable with the global increase that year.

In the NOAA air samples from Alert, an overall isotopic trend to more depleted $\delta^{13}C_{CH4}$ is apparent, beginning in about 2006 (Figure 2, bottom). Since 2008, $\delta^{13}C_{CH4}$ measurements made by RHUL and NOAA on Alert air samples show that this overall negative trend has been maintained through 2013, with a slight positive relaxation since (Figure 2, bottom, and Figure S10).

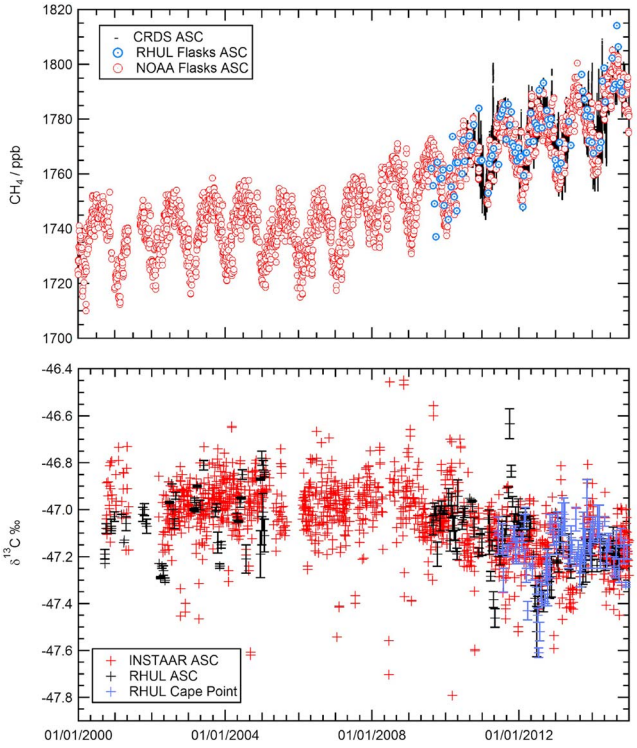

Figure 3. (top) Methane mole fraction from Airhead, Ascension Island. Red circles are NOAA discrete air samples from 2000. The black line shows RHUL continuous observations, and blue squares show RHUL flask air samples from the same site. (bottom) South Atlantic $\delta^{13}C_{CH4}$ data, 2000–2015. The graph shows both NOAA-INSTAAR (red crosses) and RHUL measurements (black crosses, showing error bars) from Ascension (ASC) and RHUL data from Cape Point, South Africa (CPT; purple crosses and error bars). See Figure S4 for trend analysis: Change in $\delta^{13}C_{CH4}$ pre-2007 was less than +0.01‰ yr^{-1}; post-2007, the shift has been in excess of −0.03‰ yr^{-1}.

3.2. Atlantic Equatorial Air—Methane and $\delta^{13}C_{CH4}$ at Ascension Island (7°58′S, 14°24′W)

At Ascension Island, strong growth in methane has been sustained from 2007 to 2014 (Figure 3, top; see also Figures S3 and S4). Taking all RHUL and NOAA measurements together, in 2010–2011 year-on-year (January to January) growth, calculated from a smoothed spline, was 10.1 ± 2.9 ppb, in contrast to the global growth rate of 5.0 ± 0.7 ppb in the NOAA data that year. In 2011–2012, an HPspline curve fit [*Pickers and Manning*, 2015] of the Ascension record shows moderate growth compared to other years (3.4 ± 1.1 ppb) and again in 2012–2013 (3.0 ± 0.9 ppb) followed by stronger growth in 2013–2014 (8.9 ± 2.7 ppb, compared to a global growth of 5.9 ± 0.5 ppb). Following 2014, very strong growth has resumed, with the year-on-year growth in monthly averages well over 10 ppb yr^{-1}. In 2014–2015, RHUL measurements show extreme growth of 12.7 ± 2.3 ppb, especially toward the end of the year (but note that at a single location, short timescale meteorological variability can have a large impact on year-on-year comparison). Further details of growth are given in the supporting information S1, section 4 and Figure S3.

In low latitudes of the Southern Hemisphere, between the equator and 30°S (i.e., southern tropics and extratropical winter rainfall belts), smoothed annual (January to January) growth trends in the NOAA network show similar behavior. In this latitudinal zone there was near-zero growth from 2001 to 2006 (including a decline in 2004 and 2005) followed by growth of 7.9 ± 0.5 ppb in 2007, 7.0 ± 0.5 ppb in 2008, 2.6 ± 0.5 ppb in 2009, 8.1 ± 0.4 ppb in 2010, 4.8 ± 0.3 ppb in 2011, 4.3 ± 0.3 ppb in 2012, 5.8 ± 0.5 ppb in 2013, and 11.2 ± 0.4 ppb in 2014.

The $\delta^{13}C_{CH4}$ record of marine boundary air sampled at Ascension Island is shown in Figure 3 (bottom). In general, methane in the Southern Hemisphere, much of which has passed through the OH-rich region in the midtroposphere around the brightly lit and humid Intertropical Convergence Zone (ITCZ), is slightly "heavier," that is, richer in ^{13}C, than north of the equator, where the dominant sources are located. Error bars in individual measurements are also shown in the figure. The data show poorly defined $\delta^{13}C_{CH4}$ isotopic seasonality and from 2001 to 2005 show no significant trend. Both NOAA and RHUL datasets independently show a shift (>0.2‰) to more ^{13}C-depleted values from 2009, becoming more marked with excursions to much more negative values in early 2011 and 2012. Values have since recovered to slightly less negative values by the end of 2014, but Ascension $\delta^{13}C_{CH4}$ values through into 2015 have stabilized around 0.2‰, more negative than in 2007–2008. This shift is far greater than experimental uncertainty (see error bars on figure). If the trends are assumed to be linear, the shift pre-2007 was less than +0.01‰ yr^{-1}; post 2007, the shift has been in excess of −0.03‰ yr^{-1} (see Figure S4). Ongoing 2015 $\delta^{13}C_{CH4}$ measurements suggest continuing decline. The assumption of a linear change in $\delta^{13}C_{CH4}$ is, however, a broad simplification.

3.3. Comparison With Other Southern Latitude Sites: Cape Point, South Africa (34°21′S, 18°30′E), and South Pole

Hybrid Single Particle Lagrangian Integrated Trajectory model (HYSPLIT) (http://www.arl.noaa.gov/HYSPLIT_info.php) [*Stein et al*., 2015] air mass backward trajectories indicate that much of the air reaching Ascension in early to mid-2012 was from the southwestern South Atlantic, including prior inputs of air from south of the equator in South America (see Figure S2), and from the Southern Ocean. From Cape Point, the RHUL flask sampling record of methane mole fraction and $\delta^{13}C_{CH4}$ (Figure 3; see also Figure S5) begins in 2011 and the NOAA record in 2009. There was moderate annual growth in mole fraction (5 ppb in 2011–2012, 3 ppb in 2012–2013) until 2013–2014, when a strong (>10 ppb) year-on-year rise took place. The RHUL $\delta^{13}C_{CH4}$ record shows a sharp shift to isotopically more negative values in 2012, reverting to previous levels in early 2013 and then perhaps becoming slightly more negative again in 2014. These Cape Point values are similar to those observed in RHUL air samples from Ascension over the same time.

Southern Hemisphere background trends are represented by NOAA samples from the South Pole (Figures S6 and S7). These measurements record strong and sustained methane growth from 2007 onward. In the polar Southern Hemisphere (60–90°S), zonal average annual means were 1726 ± 0.1 ppb in 2006, rising to 1774 ± 0.1 ppb in 2014. Concurrent with this growth is a sustained shift to more negative $\delta^{13}C_{CH4}$, also beginning around 2006 (see Figures S6 and S8). The pronounced negative dip observed at the South Pole in late 2011 is comparable to the Ascension dip in 2011 and 2012. At the South Pole, as for Ascension, if the $\delta^{13}C_{CH4}$ trends are assumed to be linear, the shift pre-2007 was negligible; post-2007, the shift has been about $-0.03‰\ yr^{-1}$ (see Figure S8).

4. Global Evolution of Trends in Methane Mole Fraction and Isotopic Values

What hypotheses can be proposed to account for these observations? In this section, possible explanations are proposed, both for the Arctic trends and for the trends observed in the savanna and equatorial tropics; then in section 5 a running budget analysis is used to investigate the hypotheses for plausibility in matching the mole fraction and isotopic records.

4.1. Possible Explanations of the Observed Growth and Isotopic Shift, Arctic and Tropical Zones

Bousquet et al. [2006] found that declining growth rates in anthropogenic emissions were the cause of the decreasing atmospheric methane growth rates during the 1990s but that after 1999 anthropogenic emissions of methane rose again. The effect of this increase was initially masked by a decrease in wetland emissions, but remote sensing data show that surface water extent started to increase again in 2002 [*Prigent et al*., 2012]. Recent widening of the Hadley Cell [*Min and Son*, 2013; *Tselioudis et al*., 2016] would have extended the high rainfall zone under the ITCZ, increasing both natural wetland and agricultural emissions in the tropics. Thus, these sources are discussed in detail, by region.

4.1.1. Arctic

The most obvious explanation of the increase in Arctic methane in 2007 is an increase in emissions. If so, isotopic and time-of-season constraints both point to increased late summer Arctic and boreal wetland emissions. Methane emitted from Arctic and boreal wetlands is markedly depleted isotopically: in Fennoscandia, atmospheric sampling and Keeling plot studies [*Fisher et al*., 2011; *Sriskantharajah et al*., 2012] showed that the emissions had $\delta^{13}C_{CH4}$ values of −70 ± 5‰, while Canadian boreal wetland emissions are around −67 ± 2‰ (unpublished RHUL studies). These values are close to the $\delta^{13}C_{CH4}$ value of around −68‰ of the regional Arctic summer methane increment over Atlantic background, indicating that the summer source is mainly from wetlands [*Sriskantharajah et al*., 2012; *Fisher et al*., 2011]. In contrast, gas field and hydrate sources are too enriched in ^{13}C to produce the observed shift. Siberian gas fields are very large but typically have $\delta^{13}C_{CH4}$ around −50 ± 3‰ [*Dlugokencky et al*., 2011], which is close to bulk atmospheric values and after dilution in regional air masses would be unlikely to produce the shift observed in the Alert values. Similarly, *Fisher et al*. [2011] and *Berchet et al*. [2016] found no evidence for large hydrate emissions.

Thus, the most likely explanation of the sharp growth in Arctic methane in late 2007, and the concurrent trend to more negative $\delta^{13}C_{CH4}$ values in ambient Arctic methane, is an increase in wetland emissions. The year 2007 was an exceptional year in the Arctic, when the North American Arctic wetlands experienced unusually sunny skies and large temperature increases compared to past records, with warm southerly winds

[*Kay et al*., 2007]. The anomalous temperatures and southerly winds [*Comiso et al*., 2008] likely drove very strong growth of summer and autumn emissions from Arctic and boreal wetlands. *Bergamaschi et al*. [2013] reported an increase in emissions of 2–3 Tg CH_4 in 2007, then below average emissions from 2008 to 2010. Similarly, *Bruhwiler et al*. [2014] estimated that in 2007, the emissions were 4.4 Tg CH_4 higher than the decadal average. The very depleted $\delta^{13}C_{CH4}$ values from Alert in autumn 2007 thus most probably record the presence of methane-rich boreal and Arctic wetland air.

From 2008 to 2013, growth of methane and isotopic shifts in the Arctic were unexceptional compared to the global record; in 2014 very strong growth occurred, but similar growth occurred elsewhere worldwide. Overall, although Arctic emissions contributed to the Arctic methane shift in 2007, they do not seem to have been major contributors since then.

4.1.2. Tropics and Southern Hemisphere: Isotopic Signatures of Sources South of 30°N

Most of the strongest growth in methane since 2007 has been led by the wider tropics, here taken as the zone between the Tropics of Cancer and Capricorn (23°26′) and also including the region experiencing passage of the Intertropical Convergence Zone (ITCZ) in South and East Asia. *Saunois et al*. [2016] found from top-down studies that almost two thirds (~64%) of the global methane emissions are from south of 30°N, while latitudes north of 60°N contribute only 4%. In the tropics, the main biogenic methane emissions are in subequatorial and savanna wetlands, from rice paddies and ruminants in southern and Southeast Asia and from ruminants in India, South America, and savanna Africa [*Kirschke et al*., 2013; *Dlugokencky et al*., 2011]; on grasslands dominated by grasses using the C4 pathway; and widespread biomass burning, especially in Africa's C4 savannas. The main anthropogenic sources in the region are not well quantified but include large ruminant populations, especially in India but also in China, Southeast Asia, South America, and Africa, in addition to dry season (winter) biomass burning. Thermogenic fossil fuel sources in the region include South Africa's coal industry, subequatorial gas fields in South America, and widespread large gas fields and coal fields in Asia and Australia.

The $\delta^{13}C_{CH4}$ values of tropical wetland methane emissions to the air (as opposed to methane within the water/vegetation/mud columns) are poorly constrained but appear typically to be around -54 ± 5‰ (unpublished RHUL results in Uganda, Southeast Asia, Peru, and Ascension; and from *Dlugokencky et al*. [2011]). This contrasts with values of around −68‰ for Arctic wetlands [*Fisher et al*., 2011]. In the northern tropics, wetland flooding from runoff is typically in the late rainy season (August–September onward) or later in river-fed swamps. Conversely, in the southern tropics (e.g., Bolivia and Zambia) wetlands fill in February–March onward. Tropical seasonal wetland emissions are readily distinguishable from dry season biomass burning emissions that come a few months later from the same general regions. Methane in smoke from grass fires in tropical C4 grasslands in winter (NH: November–February; SH: May–August) has $\delta^{13}C_{CH4}$ values around −20‰ to −10‰ (unpublished RHUL results and see supporting information S1, section 1 and *Dlugokencky et al*. [2011]). Thus, biomass burning injects methane with $\delta^{13}C_{CH4}$ that is more positive than the atmosphere: in this context, the continuing shift to negative values in 2014, an El Nino year, is of interest as such events are usually associated with biomass burning [*Duncan et al*., 2003].

The $\delta^{13}C_{CH4}$ values of tropical ruminant methane emissions have been very little studied in the field. *Schaefer et al*. [2016] assumed that ruminants are C3-fed and emit methane with $\delta^{13}C_{CH4}$ of −60‰, but grasslands and ruminant fodder crops in the tropics tend to be C4 rather than C3 dominated. *Dlugokencky et al*. [2011] considered C4 ruminant methane emissions to be -49 ± 4‰, and thus tropical ruminant emissions are likely more enriched in $\delta^{13}C_{CH4}$ than the 60‰ value assumed by *Schaefer et al*. [2016]. Many free-grazing tropical ruminants live in C4 savanna grasslands, and supplemental fodder may be maize, millet, sorghum crop waste, or sugar cane tops, all $\delta^{13}C_{CH4}$-enriched C4 plants. Thus, it is likely that methane from such cows is substantially more enriched than the −60‰ C3 value and more likely to have $\delta^{13}C_{CH4}$ values around −50‰ or less [*Dlugokencky et al*., 2011]. But tropical data are very sparse.

Fossil fuel emissions in the region south of 30°N are typically isotopically enriched in $\delta^{13}C_{CH4}$, although published isotopic measurements are few. For example, Bolivian gas in La Paz is −35‰ (unpublished RHUL results), while the very large Pars gas field in Qatar/Iran is −40‰ [*Galimov and Rabbani*, 2001]. Methane from Chinese coal is also isotopically enriched and likely to be in the −35 to −45‰ range (own observations and see *Thompson et al*. [2015]). Southern Hemisphere Gondwana coalfield methane from Australia is close to bulk atmospheric values [*Hamilton et al*., 2014], but some mines can be isotopically depleted compared to

the atmosphere [*Zazzeri et al*., 2016]. In the Hunter coalfield of Australia (typical of large coal mines in the Southern Hemisphere), *Zazzeri et al*. [2016] report $\delta^{13}C_{CH4}$ of -66.4 ± 1.3‰ from surveys around bituminous coal mines and -60.8 ± 0.3 around a ventilation shaft. Some of the more negative values may reflect the input of secondary biogenic methane into the coalfield emissions. Worldwide, open cast coal mining may be associated with the production of some isotopically lighter microbial methane.

To summarize overall, although much better site-by-site information is needed, and while emissions from a few fossil sources are isotopically relatively depleted compared to the atmosphere, methane emissions from the majority of large gas and coal fields are characteristically ^{13}C-enriched relative to the atmosphere and thus *not* the cause of the observed isotopic shifts. However, some Southern Hemisphere coalfield emissions from open cast bituminous mines may have contributed to the observed isotopic shift.

4.1.3. Ascension—The Remote Marine Tropics

Ascension lies in the heart of the southern tropics, remote from any landmass, and thus interpretation of its methane record must take note of events in the remote source regions of winds reaching the island, especially in South America (see Figure S2). The Ascension $\delta^{13}C_{CH4}$ record shows a marked change beginning in late 2010, when strong growth was accompanied by a sharp isotopic shift to more depleted $\delta^{13}C_{CH4}$, in parallel with a comparatively subdued CO cycle, albeit with excursions. The Cape Point and South Pole records are similar to the Ascension pattern (Figures 3, S5, and S6). A distant source of air reaching Ascension is Amazonia south of the ITCZ. In 2010, Amazonia experienced a major drought and biomass burning. It is possible that the early 2010 rise in methane at Ascension (Figure 3) may have been driven by biomass burning [*Crevoisier et al*., 2013], consistent with the observed enrichment of $\delta^{13}C_{CH4}$ in early to mid-2010, both typical results of C4 savanna grassland fires. However, the seasonal timing is perplexingly early in the southern winter. Trajectory studies suggest that such emissions would take some time to mix to Ascension, south of the ITCZ.

The Ascension observational record during this southern summer of 2010–2011 is most simply interpreted as the result of the very strong regional Southern Hemisphere wet season in November 2010 to March 2011, with subsequent very high Amazon flood levels in the first half of 2011 (Figure S12). Precipitation and perhaps also warmth in the wetlands may have driven a major emission pulse of isotopically strongly depleted methane during the later (wetland-filling) part of the Southern Hemisphere wet season, in March–June. This was a period so wet across the equatorial and southern tropics that ocean levels dropped [*Boening et al*., 2012]. Subsequent years were also wetter than average: record Amazon flood levels were repeatedly observed in 2012, 2013, and again in 2014, when there was heavy precipitation in the eastern flanks of the Andes in Bolivia and Peru, with exceptional flood levels in the Amazon wetlands of Bolivia in 2007, 2008, and 2014 [*Ovando et al*., 2015] (see also supporting information S1, section 12 and Figure S12). The South American tropics have experienced rising temperatures and increased wet-season precipitation post-2000 [*Gloor et al*., 2013, 2015], which would further drive increasing emissions of methane, particularly in the very hot year of 2014 [*Gedney et al*., 2004]. Wetlands in Angola, Zambia, and Botswana likely experienced also high precipitation, as evidenced by flood levels in Lake Kariba and the Okavango River in Botswana (supporting information S1, section 15).

4.1.4. Wetlands and Agriculture

Dlugokencky et al. [2009] found that the most likely drivers of methane growth in 2007–2008 were high temperatures in the Arctic and high precipitation in the tropics. In the years since then, much of the growth has a tropical geographic locus, while the isotopic evidence implies that fossil fuel emissions were not the dominant driver. This suggests that tropical wetland or agricultural emissions or a combination of both are the likely dominant causes of the global methane rise from 2008 to 2014. There is much evidence that the variations in the global methane budget are strongly dependent on tropical wetland extents and temperatures [*Bousquet et al*., 2006].

Tropical wetlands produce around 20–25% of global methane emissions: taking the mean of many models of emissions in 1993–2004 *Melton et al*. [2013] found that wetlands in the 30°N–30°S latitude belt produced 126 ± 31 Tg CH_4 yr^{-1}. Wetland methane emissions respond quickly to meteorological changes in temperature as emission has an exponential dependence on temperature [*Gedney et al*., 2004; *Westerman and Ahring*, 1987] and precipitation (expanding wetland area at the end of the rainy season). Methane emission responds rapidly to flooding and warmth [*Bridgham et al*., 2013], with lags of a few days between flooding and emission [*Chamberlain et al*., 2016], and methanogenic consortia have high resilience to drought periods.

Bousquet et al. [2016] found that variation in wetland extent could contribute 30–40% of the range of wetland emissions. Emissions show strong seasonality, following the passage of the ITCZ. Savanna wetlands fill in the late rainy seasons, after groundwater has been replenished, typically in February to April in the Southern tropics and August to October in the Northern Hemisphere tropics.

Hodson et al. [2011] showed that a large fraction of global variability in wetland emissions can be correlated with the El Niño–Southern Oscillation (ENSO) index. For example, in the La Niña years of 2007 and 2008, there is evidence that methane emissions from some Amazonian wetland regions may have increased by as much as 50% [*Dlugokencky et al*., 2009] compared to 2000–2006. Amazon flood levels (see Figure S12) were very high in 2009. In the La Niña of early 2011 [*Boening et al*., 2012], many southern tropical regions were unusually wet and equatorial Amazon flood levels were again high. Amazon flooding also took place in 2012–2014. In early 2014 (before the onset of the 2014 El Niño), extreme flood events occurred in the Amazon wetlands of Bolivia [*Ovando et al*., 2015]. Thus, summarizing, southern summer wetland (February–April) or ruminant (November–April) emissions can lead to isotopically depleted excursions, while winter (NH December–March; SH June–September) biomass burning of C4 grasslands produces CO-rich air masses with isotopically enriched methane [*Dlugokencky et al*., 2011]. The response of emissions to temperature and the lag in wetland drying may in part account for methane growth in some El Nino events (e.g., 1997), but this remains unexplained. In the moderate El Niño event of 2006, *Worden et al*. [2013] showed that methane from Indonesian fires could have compensated for an expected decrease in tropical wetland methane emissions from reduced rainfall.

Agricultural emissions also respond to high rainfall, which supports rice agriculture and fodder growth for ruminants, though widespread water storage and irrigation in the seasonal tropics is now smoothing out the impact of year-to-year fluctuations. There is no evidence for a sudden sharp increase in rice fields in 2007. Rice-harvested area in Asia is increasing but fluctuates: in 1999 (an above-trend year) the area was 140.4 million hectares and 141.0 million hectares in 2009 (a below-trend year). By 2013 Asian rice field area harvested had risen to 146.9 million hectares (http://ricestat.irri.org:8080/wrs2/entrypoint.htm). In China, as an example, it is possible that rice agriculture may have contributed to increased emissions, but there is no evidence for a step change in rice fields under cultivation: indeed, paddy field area harvested is relatively stable and declined from 2006 to 2007 (http://faostat.fao.org). Tropical agricultural emissions from ruminants are indeed likely to have increased in highly rainy seasons, but if so, these increases were probably mainly in South America and Africa. This is because in India, the nation with the world's largest ruminant population, recent monsoons have mostly been average to poor, and cattle populations have declined (see supporting information S1, section 11).

4.2. Methane Sink Variation?

A possible explanation for global methane growth is that destruction rates reduced over this time period. The global atmospheric burden of methane corresponding to 1 ppb is about 2.77 Tg of methane. Reaction with tropospheric OH is the main methane sink: for example, a 1% change in OH abundance, equivalent to a ~5 Tg CH_4 yr^{-1} change in methane emissions, or roughly 2 ppb globally, could contribute significantly to an apparent "source shift" over several years. OH abundance is greatest in the bright sunlight of the moist tropical troposphere and thus can vary significantly with short-term changes in tropical meteorology and pollution. For example, the major global wildfires during the intense El Niño event of 1997–1999 coincided with, and likely caused, an OH minimum [see *Prinn et al*., 2005; *Duncan et al*., 2003].

The long-term trend, if any, in OH abundances is not well understood [*Prinn et al*., 2005; *Patra et al*., 2014], but there is evidence for OH having small interannual variations [*Montzka et al*., 2011]. OH is well buffered in the tropical upper troposphere [*Gao et al*., 2014], and globally OH appears to have been stable within ±3% over 1985–2008: this result is more reliable from 1997 onward [*Rigby et al*., 2008]. *Rigby et al*. [2008] inferred a large, but uncertain, decrease in OH in 2007 ($-4 \pm 14\%$), implying that part of the growth in methane mole fraction in 2007 may have been driven by a smaller sink; however, that work had not considered the isotopic CH_4 data. During 2006–2008, OH may have only varied by less than 1% globally, although larger regional changes may have occurred, with some evidence for low OH over the western Pacific warm pool [*Rex et al*., 2014]. Thus, there is little prima facie evidence that a major change in OH has driven methane's rise and isotopic shift. Methane removal by the atomic Cl sink, discussed in supporting information S1, section 16, is also unlikely to explain the observed changes.

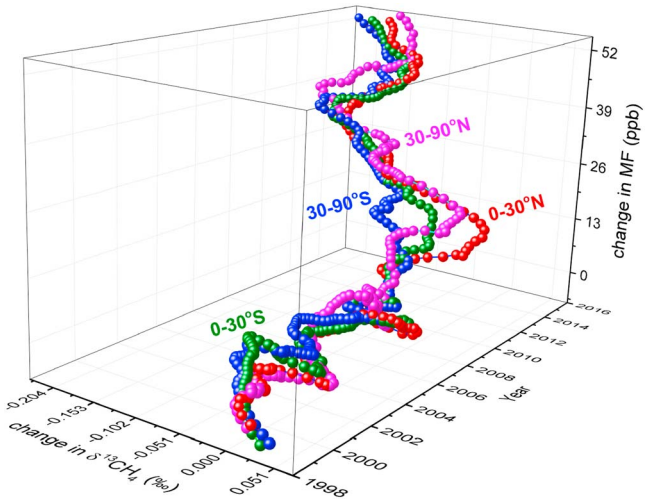

Figure 4. Three-dimensional graphic for changes in $\delta^{13}C_{CH4}$ and mole fraction with time, showing midpoints for the years marked. MF = mole fraction. Color code: blue = 30–90°S, green = 0–30°S, red = 0–30°N, mauve = 30–90°N.

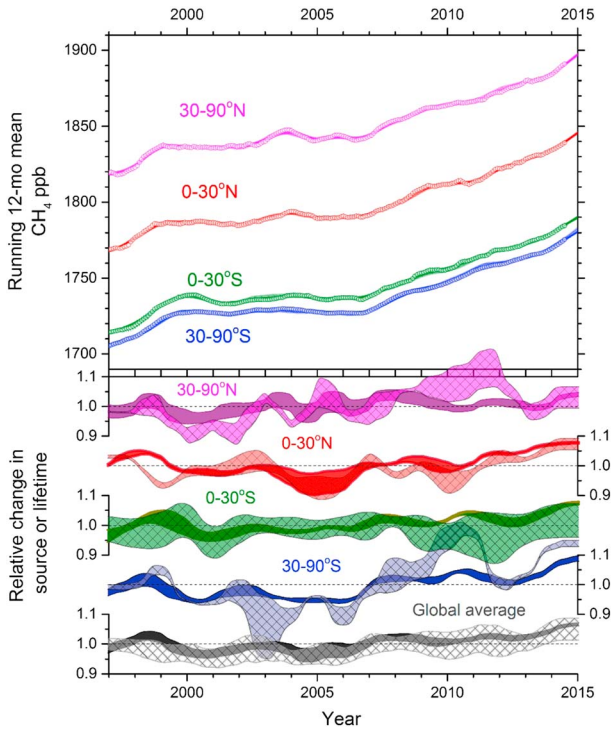

Figure 5. (top) Running 12 month means of methane mole fractions from the NOAA Cooperative Global Air Sampling Network averaged over 0–30° and 30–90° latitude regions in each hemisphere (see supporting information S1, section 16). Uncertainty bands around these running means show the range of mole fraction values that remain after correcting for average site differences. Ranges for fits to the data are shown using changes either in CH_4 source emissions (darker) or in removal rates (lighter); however, as each gives good fits to the mole fractions these are hard to distinguish. (bottom) The corresponding ranges for relative changes in zonal CH_4 source emissions (darker) or lifetimes, i.e., the inverse of removal rates (lighter and crosshatched) for each region and for the global average. See text for source emission and removal rate ranges.

5. Running Budget Analysis and Interpretation of Shifts in the $\delta^{13}C_{CH4}$ Record

An objective analysis of the cause for the recent rise in methane requires a balanced consideration of changes in sources or removal rates. Figure 4 summarizes the changes with time of mole fraction and $\delta^{13}C_{CH4}$ over the period since 1998. The importance of $\delta^{13}C_{CH4}$ data for identifying such changes in CH_4 sources or removal rates is becoming increasingly clear [*Monteil et al.*, 2011; *Ghosh et al.*, 2015].

To consider how the most recent data can clarify explanations for the increase in mole fraction together with the striking concurrent reversal of the long-term trend for increasing $\delta^{13}C_{CH4}$ over the last hundred years, a latitudinally zoned monthly budget analysis is carried out here. Two hypotheses to explain the recent changes in the methane mole fraction and isotopic records are considered: (a) "changes in emissions" or (b) "changes in removal rates." The second option also considers whether a spatial redistribution of removal rates can explain the recent changes in atmospheric CH_4.

There are still significant uncertainties in the CH_4 budget, as shown by the bottom-up estimates for emissions from natural sources over 2000–2009 being 50% larger than their top-down estimates and the range of estimates for anthropogenic emissions being 100% larger for top-down estimates than for bottom-up estimates [*Ciais et al.*, 2013]. However, the focus here is to consider how recent changes in the budget can cause a transition from the relatively stable period over 1999–2006 to significant increases in mole fraction together with decreases in $\delta^{13}C_{CH4}$ over 2007–2014. This is done by considering the magnitudes and timings of changes to a central estimate for the top-down budget [*Kirschke et al.*, 2013; *Ciais et al.*, 2013] which can explain the observations. This is not designed to improve our understanding of the total budget

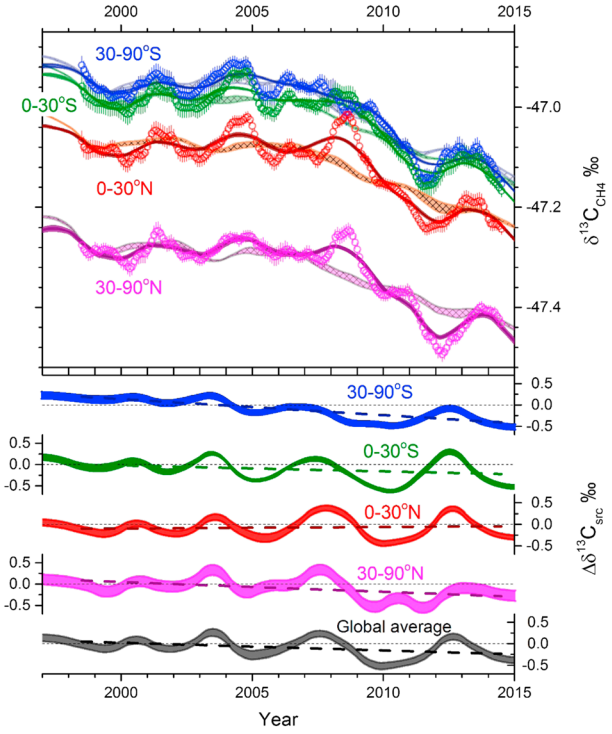

Figure 6. (top) Running 12 month means for $\delta^{13}C_{CH4}$ from the NOAA and RHUL sites that have also been combined to represent averages over the four regions. Results from the budget analysis are shown for changes in source emissions (darker) or removal rates (lighter and crosshatched) as in Figure 5. (bottom) The corresponding variations in source $\delta^{13}C$ (‰) for the four regions and for the global average source $\delta^{13}C$.

but rather to assess how much it has to change to explain recent data.

A simple running budget analysis is used here to compare how variations in CH_4 emissions or in its removal rate can explain the observed changes in mole fraction and $\delta^{13}C_{CH4}$ data. The focus is on 1998–2014. However, NOAA mole fraction data from 1983, together with ice core and firn air data [*Ferretti et al.*, 2005], and earlier NIWA (New Zealand National Institute of Water and Atmospheric Research) $\delta^{13}C_{CH4}$ data over 1992–1997 [*Lassey et al.*, 2000] have also been used to carry out a spin-up phase for this analysis.

Monthly average mole fraction and $\delta^{13}C_{CH4}$ data are used to determine the total emissions and their $\delta^{13}C$ values for four semihemisphere regions (30–90°S, 0–30°S, 0–30°N, and 30–90°N) but with the focus being on long-term trends and major year-to-year variations around these, rather than specific regional effects. CH_4 mixes within each hemisphere over periods of a few months and between hemispheres over about 1 year. As shown in Figures S13 and S14, this leads to a fairly stable spatial distribution modulated by seasonal cycles that depend on location but have relatively small interannual variations [*Dlugokencky et al.*, 1994]. Cubic spline fits to the CH_4 data for the four regions are then used to compare how monthly variations in emissions or in removal rates can reproduce the data over 1998–2014.

Interannual variations are shown by using running 12 month means to remove the seasonal cycle for the observed mole fraction data in Figure 5 and for $\delta^{13}C_{CH4}$ in Figure 6. However, the budget analysis is fitted to monthly data, as shown in supporting information S1, section 16, in order to cover seasonal cycles in emissions and removal rates that have nonlinear effects on isotope ratios.

The differential equations used here to relate mole fractions to emissions and removal rates are

$$\frac{\mathrm{d}}{\mathrm{d}t}C_i = S_i - K_i C_i - \sum\nolimits_j X_{ij}\left(C_i - C_j\right) \tag{1}$$

where i denotes a region, C_i are mole fractions in units of ppb, S_i are emission rates in units of ppb/yr, K_i are removal rates (1/yr), and X_{ij} are exchange rates between the one or two adjacent regions. The differential equations used for $\delta^{13}C_{CH4}$ are similar to *Lassey et al.* [2000] where simpler differential equations for $^{13}C/C$, are treated by using systematic differences between $^{13}C/^{12}C$ and $^{13}C/C$ ratios as

$$\left[{}^{13}CH_4\right] = (1+\delta)R_{PDB}\left[{}^{12}CH_4\right] = \frac{(1+\delta)R_{PDB}}{\left[1+(1+\delta)R_{PDB}\right]}C_i = \left(1+\delta'\right)R_{PDB}C_i \tag{2}$$

where $R_{PDB} = 0.0112372$ for the VPDB (Vienna Pee Dee Belemnite) standard, and δ' applies to the $^{13}C/C$ ratios. The differential equations for $^{13}CH_4$ mole fractions, now written as F_i, are then

$$\frac{\mathrm{d}}{\mathrm{d}t}F_i = \left(1+\delta'_{Si}\right)R_{PDB}S_i - (1+\varepsilon)K_i\left(1+\delta'_i\right)R_{PDB}C_i - \sum\nolimits_j X_{ij}\left(F_i - F_j\right) \tag{3}$$

Table 1. The Range of Options Considered in Determining Fits of Sources or of Removal Rates to the Regional Mole Fraction and $\delta^{13}C_{CH4}$ Data

Process	Option 1	Option 2
	Seasonal Cycles	
OH removal	*Spivakovsky et al.* [2000]	
Cl removal	Constant	Same as OH
Soil removal	Constant	Same as OH
Cross tropopause transport	Constant	
Source	Fitted to data for each region, no interannual variability	
Source $\delta^{13}C$	Fitted to data for each region, no interannual variability	
	Spatial Distributions	
OH removal	*Spivakovsky et al.* [2000]	
Cl removal	Uniform	SH only
Soil removal	Proportional to land area	
Cross tropopause transport	Uniform	Low latitudes only
	Interannual Variations	
	Source fits	Removal rate fits
Removal rates	No change	Vary over 1992–2014
Source	Vary over 1990–2014	Vary over 1990–1998
Source $\delta^{13}C_S$	Vary over 1998–2014	Vary over 1990–1998
Exchange rates 1990–2014	Fixed varying	Fixed varying

where δ'_{Si} are for the source $^{13}C/C$ ratios, and ε is the Kinetic Isotope Effect for the removal rate. This can then be simplified to

$$\frac{d}{dt}\delta'_i = \left(\delta'_{Si} - \delta'_i\right)(S_i/C_i) - \varepsilon K_i - \sum\nolimits_j X_{ij}\left(\delta'_i - \delta'_j\right)(C_j/C_i) \quad (4)$$

While equation (1) and its equivalent for [$^{13}CH_4$] used in some analyses [*Schaefer et al.*, 2016] are linear equations, (4) makes it clear that the δ_i' have nonlinear relationships with the S_i and C_i.

Mole fraction data from 51 NOAA sites together with $\delta^{13}C_{CH4}$ data from 20 NOAA sites and 2 RHUL sites are used, but because of limited spatial coverage for $\delta^{13}C_{CH4}$ data, monthly averages over four semihemispheres, covering 0–30° and 30–90° zonal regions, are used to determine corresponding emissions, removal, and transport. The CH_4 emissions and their $\delta^{13}C$ values are fitted to the observed mole fraction and $\delta^{13}C_{CH4}$ data using a range of estimates for removal rates consistent with the last IPCC (Intergovernmental Panel on Climate Change) assessment report [*Ciais et al.*, 2013] but covering options for spatial and seasonal distributions of the removal by soils, tropospheric Cl, and cross tropopause transport which are less well defined than they are for removal by OH. Interannual variations in exchange rates between the regions are also considered as another option. Then for comparison an alternative set of model runs allows interannual variations in the removal rate over 1998–2014 while keeping the emissions fixed after 1999. In both cases this is a simple form of inverse modeling that avoids prior estimates of the source budget and treats interannual variations in either source emissions or in removal rates equally. More details of the data averaging and running budget analysis are provided in Table 1 and in supporting information S1, section 16.

5.1. Mole Fraction Constraints

Most of the variation in mole fraction data can be explained by either of the two hypotheses: "changes in source emissions," or "changes in removal rates", or a combination of both. Models assuming changes in emissions only and "changes in removals" only are shown in Figure 5. While there are some systematic differences between data and fits, the residuals are only slightly larger for the changes in removal option.

The changes in source emissions model shown in Figure 5 has emissions in the range 560–580 Tg CH_4 yr^{-1} when averaged over 1998–2014, similar to values of *Kirschke et al.* [2013], with 11% in the 30–90°S region, 27% in 0–30°S, 32% in 0–30°N, and 30% in 30–90°N. There is a source trend of 0.8 to 1.5% yr^{-1} in the 0–30°N region over 2005 to 2014 in contrast to the 30–90°N that has a trend of −0.5 to +0.1% yr^{-1} over this period. In the 0–30°S region this trend is 0.4 to 0.5% yr^{-1}, and in the 30–90°S region it is 0.8 to 0.9% yr^{-1}. The larger relative variations for 30–90°S may reflect this zone's emissions being small relative to the global total

making it more sensitive to variations in transport such as an increasing extent of Hadley circulation [*Tselioudis et al*., 2016]. Total source increases over this period are in the range of 3 to 6% and predominantly in the 0–30°S and 0–30°N regions. These source changes are described in more detail in supporting information S1, section 16 and are consistent with other estimates [*Dlugokencky et al*., 2009; *Bousquet et al*., 2011] but have now been continuing for 9 years.

If, alternatively, changes in removal rates (or lifetimes) are used to explain the CH_4 mole fraction data, then significantly larger relative variations are needed than for source variations; however, this is partly due to the constraints also being imposed by the $\delta^{13}C_{CH4}$ data as shown below. Over 1998–2014, variations of 7%–10% are used in the low latitudes and 15%–25% in the high latitudes. In particular, the slowdown in CH_4 growth rate over 2009–2011 requires very large increases in the lifetimes in high latitudes and some compensating reduction in lifetimes in the low latitudes. Relative changes in the global mean lifetime are smaller because of these compensating effects, but it still requires an increase of ~10% over 2000–2014. This is much larger than expected fluctuations of OH radicals [*Montzka et al*. 2011]. Furthermore, because cross tropopause transport is expected to remove ~8% of CH_4 while reaction with Cl and the soil sink each account for 4–5% [*Ciais et al*., 2013], variations in removal rate that are required to explain the observed mole fraction data cannot be explained without some significant changes in OH.

5.2. Isotopic Constraints

An even clearer distinction between the two modeled hypotheses is shown when isotopes are considered (Figure 6). The shift in the bulk $\delta^{13}C_{CH4}$ value of the global source is about −0.17‰. The changes in source emissions option follows the interannual variations in $\delta^{13}C_{CH4}$ much better than the changes in removal rates option and this is more obvious in the Northern Hemisphere where these variations are large. Furthermore, variations in removal rates cannot explain the large positive anomalies in 2004 and 2008 or the large negative anomaly over 2011–2012.

Source $\delta^{13}C$ values averaged over 1998–2014 for the regions are in the following ranges: -57.8 ± 0.05‰ for 30–90°S; -53.9 ± 0.04‰ for 0–30°S; -51.9 ± 0.07‰ for 0–30°N; and -53.4 ± 0.13‰ for 30–90°N. In addition to significant interannual variations mentioned above there is also clearly a longer-term trend of decreasing $\delta^{13}C_{CH4}$ values. Figure 6 shows that this corresponds to a decrease in source $\delta^{13}C$ values that started 5 to 10 years earlier as would be expected because of the significant lag in the $\delta^{13}C_{CH4}$ response to change [*Tans*, 1997]. The most obvious trends in source $\delta^{13}C$ are in the 30–90°S and 30–90°N regions, but there is also a negative trend in the 0–30°S region (see also Figure S4). This spatial pattern for trends in source isotopic signatures may relate to the long-term decrease in biomass burning over this period [*Le Quéré et al*., 2014] at the same time as an increase in wetland emissions [*Bousquet et al*., 2011]. Also, the timing for this change in source $\delta^{13}C$ values is consistent with satellite data showing trends in land surface open water areas that decreased from 1993 to 2002 but then started to increase [*Prigent et al*., 2012].

While an increase in lifetimes, i.e., decrease in removal rates by OH and other sinks, could reproduce the long-term decrease in $\delta^{13}C_{CH4}$, this analysis shows that it requires major changes in the global average removal rate as well as large fluctuations in the four semihemispheres, while still not accounting for much of the year-to-year interannual variations. The extent to which reversal of the long-term trend in $\delta^{13}C_{CH4}$ could be caused by a decrease in OH is heavily constrained by the more direct tracers of OH which suggest that it has no long-term trend [*Montzka et al*., 2011]. However, a much larger fractionation occurs in removal by soil methanotrophy, and this can be anticorrelated with methanogenesis [*Bridgham et al*., 2013] so that changes in wetlands could be having a larger relative effect on the seasonal cycle for $\delta^{13}C_{CH4}$ than for the mole fraction. Furthermore, the large isotopic fractionation due to reaction with Cl in the marine boundary layer is sensitive to temperature, and this may lead to interannual variability that may have been recognized in some data not included here [*Allan et al*., 2001].

6. Conclusions

The $\delta^{13}C_{CH4}$ isotopic shifts reported here and the likelihood that changes in the OH methane sink are not consistent with the observed trends suggest that from 2007 growth in atmospheric methane has been largely driven by increased biogenic emissions of methane, which is depleted in ^{13}C. Both the majority of this methane increase and the isotopic shift are biogenic. This growth has been global but, apart from 2007, has

been led from emissions in the tropics and Southern Hemisphere, where the isotopically depleted biogenic sources are primarily microbial emissions from wetlands and ruminants, with the trend in source $\delta^{13}C_{CH4}$ in the 0–30°S zone being particularly interesting.

While significant uncertainties in the global methane budget still remain, our top-down analysis has shown that relative increases in the global average emissions of 3–6% together with a shift of about −0.17‰ in the bulk $\delta^{13}C_{CH4}$ value of the global source over the last 12 years can explain much of the observed trends in methane's mole fraction and $\delta^{13}C_{CH4}$ values. Alternative explanations, such as increases in the global average atmospheric lifetime of methane, would have to have been an unrealistic 5–8% over this period and cannot explain the interannual variations observed in $\delta^{13}C_{CH4}$.

Although fossil fuel emissions have declined as a proportion of the total methane budget, our data and results cannot rule out an increase in absolute terms, especially if the source gas were isotopically strongly depleted in ^{13}C: however, both the latitudinal analysis and isotopic constraints rule out Siberian gas, which is around −50‰ [*Dlugokencky et al*., 2011], as a cause of the methane rise, and emissions from other fossil fuel sources such as Chinese coal, US fracking, or most liquefied natural gas are typically more enriched in ^{13}C and thus also do not fit the isotopic constraints.

The evidence presented here, and in the supporting information, is that the growth, isotopic shift, and geographic location coincide with the unusual meteorological conditions of the past 9 years, especially in the tropics. These events included the extremely warm summer and autumn in 2007 in the Arctic, the intense wet seasons in the Southern Hemisphere tropics under the ITCZ in late 2010–2011 and subsequent years, and also the very warm year of 2014. The monsoonal 0°–30°N Northern Hemisphere, probably especially in South and East Asia [*Nisbet et al*., 2014; *Patra et al*., 2016], also contributed to post-2011 growth.

Schaefer et al. [2016], using a one-box model, considered but rejected the hypothesis that wetland emissions have been the primary cause of methane growth. This was on the basis of remote sensing data that suggested that growth was led from the Northern Hemisphere and also isotopic arguments, as they assumed that tropical ruminants were C3-fed. They preferred the hypothesis that growth has been driven by agricultural emissions but commented that the evidence was "not strong." The evidence presented here for the latitudinal distribution of growth suggests that Southern Hemisphere wetland emissions may have been more important than thought by *Schaefer et al*. [2016].

Our study concurs with *Schaefer et al*. [2016] that the methane rise is a result of increased emissions from biogenic sources. The location and strong interannual variability of the methane growth suggest that a fluctuating natural source is predominant rather than an anthropogenic one. Rice field and ruminant emissions have likely contributed significantly to the rise in tropical methane emissions, but rice-harvested areas and animal populations change slowly and there is little evidence for a step change in 2007 that is capable of explaining the trend change in the methane record. Consequently, while agricultural emissions are likely to be increasing, as postulated by *Schaefer et al*. [2016], and probably have been an important component in the recent increase, we find that tropical wetlands are likely the dominant contributor to recent growth.

Schaefer et al. [2016] raised the troubling concern that the need to control methane emissions may conflict with food production. They warned that, "if so, mitigating CH_4 emissions must be balanced with the need for food production." This is a valid concern, but we believe that changes in tropical precipitation and temperature may be the major factors now driving methane growth, both in natural wetlands and in agriculture.

Renewed growth in atmospheric methane has now persisted for 9 years. The methane record from 1983 to 2006 (Figure 1) shows a clear trend to steady state [*Dlugokencky et al*., 2009; *Dlugokencky et al*., 2011], apart from "one-off" events, such as the impact of the Pinatubo eruption in 1991–1992 and the intense El Niño of 1997–1998. But the current growth is different and has been sustained since 2007, although the modeling work presented above suggests that the present trend to more isotopically depleted values may have started in the last years of the previous century. The abrupt timing of the change in growth trend in 2007 is consistent with a hypothesis that the growth change was primarily in response to meteorological driving factors. Changes in emissions from anthropogenic sources, such as fossil fuels, agricultural ruminant populations, and area of rice fields under cultivation, would be more gradual. The strong isotopic shifts measured in late

2010–2011 are consistent with a response to the intense La Niña. The exceptional global methane increase in 2014 (Figure 1) was accompanied by a continuation of the recent isotopic pattern (Figures 2, 3, and S10).

The scale and pace of the present methane rise (roughly 60 ppb in 9 years since the start of 2007), and the concurrent isotopic shift showing that the increase is dominantly from biogenic sources, imply that methane emission (both from natural wetlands and agriculture) is responding to sustained changes in precipitation and temperature in the tropics. If so, is this merely a decadal-length weather oscillation, or is it a troubling harbinger of more severe climatic change? Is the current sustained event in the normal range of meteorological fluctuation? Or is a shift occurring that is becoming comparable in scale to events recorded in ice cores [*Wolff and Spahni*, 2007; *Möller et al*., 2013; *Sperlich et al*., 2015]? In the past millennium between 1000 and 1700 C.E., methane mole fraction varied by no more than about 55 ppb [*Feretti et al*., 2005]. Methane in past global climate events has been both a "first indicator" and a "first responder" to climatic change [*Severinghaus and Brook*, 1999; *Möller et al*., 2013; *Etheridge et al*., 1998]. Comparison with these historic events suggests that if methane growth continues, and is indeed driven by biogenic emissions, the present increase is already becoming exceptional, beyond the largest events in the last millennium.

Acknowledgments

This work was supported by the UK NERC projects NE/N016211/1 The Global Methane Budget, NE/M005836/1 Methane at the edge, NE/K006045/1 The Southern Methane Anomaly and NE/I028874/1 MAMM. We thank the UK Meteorological Office for flask collection and hosting the continuous measurement at Ascension, the Ascension Island Government for essential support, and Thumeka Mkololo for flask collection in Cape Town. Data sources and archiving are listed in the supporting information S1, section 2. RHUL data are being stored with the UK Centre for Environmental Data Analysis. NOAA data are accessible from ftp://aftp.cmdl.noaa.gov/data/greenhouse_gases/ch4/flask/surface/. For figures, see the U.S. NOAA ESRL website and http://www.esrl.noaa.gov/gmd/ccgg/figures/. INSTAAR data found in the readme file are available from ftp://aftp.cmdl.noaa.gov/data/trace_gases/ch4c13/flask/surface/ and ftp://aftp.cmdl.noaa.gov/data/trace_gases/ch4c13/flask/surface/README_surface_flask_ch4c13.html

References

Allan, W., M. R. Manning, K. R. Lassey, D. C. Lowe, and A. J. Gomez (2001), Modelling the variation of $\delta^{13}C$ in atmospheric methane: Phase ellipses and the kinetic isotope effect, *Global Biogechem. Cycles*, *15*(2), 467-481, doi:10.1029/2000GB001282.

Berchet, A., et al. (2016), Atmospheric constraints on the methane emissions from the East Siberian Shelf, *Atmos. Chem. Phys.*, *16*, 4147–4157.

Bergamaschi, P., et al. (2013), Atmospheric CH_4 in the first decade of the 21st century: Inverse modeling analysis using SCIAMCHY satellite retrievals and NOAA surface measurements, *J. Geophys. Res. Atmos.*, *118*, 7350–7369, doi:10.1002/jgrd.50480.

Boening, C., J. K. Willis, F. W. Landerer, R. S. Nerem, and J. Fasullo (2012), The 2011 La Niña: So strong the oceans fell, *Geophys. Res. Lett.*, *39*, L19602, doi:10.1029/2012GL053055.

Bousquet, P., et al. (2006), Contribution of anthropogenic and natural sources to atmospheric methane variability, *Nature*, *443*, 439–443.

Bousquet, P., et al. (2011), Source attribution of the changes in atmospheric methane for 2006–2008, *Atmos. Chem. Phys.*, *11*, 3689–3700.

Bridgham, S. D., H. Cadillo-Quiroz, J. K. Keller, and Q. Zhuang (2013), Methane emissions from wetlands: Biogeochemical, microbial, and modeling perspectives from local to global scales, *Global Change Biol.*, *19*, 1325–1346.

Bruhwiler, L. M., E. Dlugokencky, K. Masarie, M. Ishizawa, A. Andrews, J. Miller, C. Sweeney, P. Tans, and D. Worthy (2014), CarbonTracker-CH_4: An assimilation system for estimating emissions of atmospheric methane, *Atmos. Chem. Phys.*, *14*, 8269–8293.

Chamberlain, S. D., N. Gomez-Casanovas, M. T. Walter, E. H. Boughton, C. J. Bernacchi, E. H. DeLucia, P. M. Groffman, E. W. Keel, and J. P. Sparks (2016), Influence of transient flooding on methane fluxes from sub-tropical pastures, *J. Geophys. Res. Biogeosci.*, *121*, 965–977, doi:10.1002/2015JG003283.

Ciais, P., et al. (2013), Chapter 6: Carbon and other biogeochemical cycles, in *Working Group I Contribution to the IPCC Fifth Assessment Report (AR5), Climate Change 2013: The Physical Science Basis*, edited by T. Stocker et al., Cambridge University Press, Cambrige.

Comiso, J. C., C. L. Parkinson, R. Gersten, and L. Stock (2008), Accelerated decline in the Arctic sea ice cover, *Geophys. Res. Lett.*, *35*, L01703, doi:10.1029/2007GL031972.

Crevoisier, C., et al. (2013), The 2007–2011 evolution of tropical methane in the mid-troposphere as seen from space by MetOp-A/IASI, *Atmos. Chem. Phys.*, *13*, 4279–4289.

Dlugokencky, E. J., K. A. Masarie, P. M. Lang, P. P. Tans, L. P. Steele, and E. G. Nisbet (1994), A dramatic decrease in the growth rate of atmospheric methane in the northern hemisphere during 1992, *Geophys. Res. Lett.*, *21*, 45–8.

Dlugokencky, E. J., K. A. Masarie, P. M. Lang, and P. P. Tans (1998), Continuing decline in the growth rate of atmospheric methane, *Nature*, *393*, 447–450.

Dlugokencky, E. J., R. C. Myers, P. M. Lang, K. A. Masarie, A. M. Crotwell, K. W. Thoning, B. D. Hall, J. W. Elkins, and L. P. Steele (2005), Conversion of NOAA atmospheric dry air CH_4 mole fractions to a gravimetrically prepared standard scale, *J. Geophys. Res.*, *110*, D18306, doi:10.1029/2005JD006035.

Dlugokencky, E. J., et al. (2009), Observational constraints on recent increases in the atmospheric CH_4 burden, *Geophys. Res. Lett.*, *36*, L18803, doi:10.1029/2009GL039780.

Dlugokencky, E. J., E. G. Nisbet, R. E. Fisher, and D. Lowry (2011), Global atmospheric methane: Budget, changes, and dangers, *Philos. Trans. R. Soc. London, Ser. A.*, *369*, 2058–2072.

Duncan, B. N., R. V. Martin, A. C. Staudt, R. Yevich, and J. A. Logan (2003), Interannual and seasonal variability of biomass burning emissions constrained by satellite observations, *J. Geophys. Res.*, *108*(D2), 4040, doi.10.1029/2002JD002378.

Etheridge, D. M., L. P. Steele, R. J. Francey, and R. L. Langenfels (1998), Atmospheric methane between 1000 A.D. and present: Evidence of anthropogenic emissions and climatic variability, *J. Geophys. Res.*, *103*, 15,979–15,993, doi:10.1029/98JD00923.

Ferretti, D. F., et al. (2005), Unexpected changes to the global methane budget over the past 2000 years, *Science*, *309*, 1714.

Fisher, R. E., et al. (2011), Arctic methane sources: Isotopic evidence for atmospheric inputs, *Geophys. Res. Lett.*, *38*, L21803, doi:10.1029/2011GL049319.

Galimov, E. M., and A. R. Rabbani (2001), Geochemical characteristics and origin of natural gas in southern Iran, *Geochem. Int.*, *39*, 780–792.

Gao, R. S., K. H. Rosenlof, D. W. Fahey, P. O. Wennberg, E. J. Hintsa, and T. F. Hanisco (2014), OH in the tropical upper troposphere and its relationships to solar radiation and reactive nitrogen, *J. Atmos. Chem.*, *71*, 55–64.

Gedney, N., P. M. Cox, and C. Huntingford (2004), Climate feedback from wetland methane emissions, *Geophys. Res. Lett.*, *31*, L20503, doi:10.1029/2004GL020919.

Ghosh, A., et al. (2015), Variations in global methane sources and sinks during 1910–2010, *Atmos. Chem. Phys.*, *15*, 2595–2612.

Gloor, M., R. J. W. Brienen, D. Galbraith, T. R. Feldpausch, J. Schöngart, J.-L. Guyot, J. C. Espinoza, J. Lloyd, and O. L. Phillips (2013), Intensification of the Amazonian hydrological cycle over the last two decades, *Geophys. Res. Lett.*, *40*, 1729–1733, doi:10.1002/grl.50377.

Gloor, M., J. Barichivich, G. Ziv, R. Brienen, J. Schöngart, P. Peylin, B. B. Ladvocat Cintra, T. Feldpausch, O. Phillips, and J. Baker (2015), Recent Amazon climate as background for possible ongoing and future changes of Amazon humid forests, *Global Biogeochem. Cycles*, *29*, 1384–1399, doi:10.1002/2014GB005080.

Hamilton, S. K., S. D. Golding, K. A. Baublys, and J. S. Esterle (2014), Stable isotopic and molecular composition of desorbed coal seam gases from the Walloon Subgroup, eastern Surat Basin, Australia, *Int. J. Coal Geol.*, *122*, 21–36.

Hodson, E. L., B. Poulter, N. E. Zimmermann, C. Prigent, and J. O. Kaplan (2011), The El Niño-Southern Oscillation and wetland methane interannual variability, *Geophys. Res. Lett.*, *38*, L08810, doi:10.1029/2011GL046861.

Kay, J. E., T. L'Ecuyer, A. Gettelman, G. Stephens, and C. O'Dell (2007), The contribution of cloud and radiation anomalies to the 2007 Arctic Sea Ice minimum, *Geophys. Res. Lett.*, *35*, L08503, doi:10.1029/2008GL033451.

Kirschke, S., et al. (2013), Three decades of global methane sources and sinks, *Nat. Geosci.*, *6*, 813–823.

Lassey, K. R., D. C. Lowe, and M. R. Manning (2000), The trend in atmospheric methane $\delta^1$3C and implications for isotopic constraints on the global methane budget, *Global Biogeochem. Cycles*, *14*, 41–49.

Le Quéré, C., et al. (2014), Global carbon budget 2013, *Earth Syst. Sci. Data*, *6*, 235–263.

Melton, J. R., et al. (2013), Present state of global wetland extent and wetland methane modeling: Conclusions from a model intercomparison project (WETCHIMP), *Biogeosciences*, *10*, 753–788.

Min, S.-K., and S.-W. Son (2013), Multimodal attribution of the Southern Hemisphere Hadley cell widening: Major role of ozone depletion, *J. Geophys. Res. Atmos.*, *118*, 3007–3015, doi:10.1002/jgrd.50232.

Möller, L., T. Sowers, M. Bock, R. Spahni, M. Behrens, J. Schmitt, H. Miller, and H. Fischer (2013), Independent variations of CH_4 emissions and isotopic composition over the past 160,000 years, *Nat. Geosci.*, *6*, 885–890.

Monteil, G., S. Houweling, E. J. Dlugockenky, G. Maenhout, B. H. Vaughn, J. W. C. White, and T. Rockmann (2011), Interpreting methane variations in the past two decades using measurements of CH_4 mixing ratio and isotopic composition, *Atmos. Chem. Phys.*, *11*, 9141–9153.

Montzka, S. A., M. Krol, E. Dlugokencky, B. Hall, P. Jöckel, and J. Lelieveld (2011), Small interannual variability of global atmospheric hydroxyl, *Science*, *331*, 67–69.

Nisbet, E. G., E. J. Dlugokencky, and P. Bousquet (2014), Methane on the rise – Again, *Science*, *343*, 493–5.

Ovando, J., J. Tomasella, D. A. Rodriguez, J. M. Martinez, J. L. Siqueira-Junior, G. L. N. Pinto, P. Passy, P. Vauchel, L. Noriega, and C. von Randow (2015), Extreme flood events in the Bolivian Amazon wetlands, *J. Hydrol. Reg. Stud.*, *5*, 293–308.

Patra, P. K., et al. (2014), Observational evidence for inter-hemispheric hydroxyl-radical parity, *Nature*, *513*, 219–223.

Patra, P. K., et al. (2016), Regional methane emission estimation based on observed atmospheric concentrations (2002–2012), *J. Met. Soc. Jpn.*, *94*, 91–113.

Pickers, P. A., and A. C. Manning (2015), Investigating bias in the application of curve fitting programs to atmospheric time series, *Atmos. Meas. Tech.*, *8*, 1469–1489.

Prigent, C., F. Papa, F. Aires, C. Jiménez, W. B. Rossow, and E. Matthews (2012), Changes in land surface water dynamics since the 1990s and relation to population pressure, *Geophys. Res. Lett.*, *39*, L08403, doi:10.1029/2012GL051276.

Prinn, R. G., et al. (2005), Evidence for variability of atmospheric hydroxyl radicals over the past quarter century, *Geophys. Res. Lett.*, *32*, L07809, doi:10.1029/2004GL022228.

Rex, M., et al. (2014), A tropical West Pacific OH minimum and implications for stratospheric composition, *Atmos. Chem. Phys.*, *14*, 4827–4841.

Rigby, M., et al. (2008), Renewed growth of atmospheric methane, *Geophys. Res. Lett.*, *35*, L22805, doi:10.1029/2008GL036037.

Saunois, M., et al. (2016), The Global Methane budget: 2000–2012, *Earth Syst. Sci. Data Discuss.*, doi:10.5194/essd-2016-25.

Schaefer, H., et al. (2016), A 21st century shift from fossil-fuel to biogenic methane emissions indicated by $13CH_4$, *Science*, *352*, 80–84.

Severinghaus, J. P., and E. J. Brook (1999), Abrupt climate change at the end of the last glacial period inferred from trapped air in polar ice, *Science*, *286*, 930–934.

Sperlich, P., H. Schaefer, S. E. Mikaloff Fletcher, M. Guillevic, K. Lassey, C. J. Sapart, T. Röckmann, and T. Blunier (2015), Carbon isotope ratios suggest no additional methane from boreal wetlands during the rapid Greenland Interstadial 21.2, *Global. Biogeochem. Cycles*, *29*, 1962–1976, doi:10.1002/2014GB005007.

Spivakovsky, C. M., et al. (2000), Three dimensional climatological distribution of tropospheric OH: Update and evaluation, *J. Geophys. Res.*, *105*, 8931–8980, doi:10.1029/1999JD901006.

Sriskantharajah, S., R. E. Fisher, D. Lowry, T. Aalto, J. Hatakka, M. Aurela, T. Laurila, A. Lohila, E. Kuitunen, and E. G. Nisbet (2012), Stable carbon isotope signatures of methane from a Finnish subarctic wetland, *Tellus B*, *64*, 18818.

Stein, A. F., R. R. Draxler, G. D. Rolph, B. J. B. Stunder, M. D. Cohen, and F. Ngan (2015), NOAA'S HYSPLIT Atmospheric Transport and Dispersion Modeling System, *Bull. Am. Meteorol. Soc.*, *96*, 2059–2077, doi:10.1175/bams-d-14-00110.1.

Tans, P. P. (1997), A note on isotopic ratios and the global atmospheric methane budget, *Global Biogeochem. Cycles*, *11*, 77–81, doi:10.1029/96GB03940.

Thompson, R. L., et al. (2015), Methane emissions in East Asia for 2000–2011 estimated using an estimated Bayesian inversion, *J. Geophys. Res. Atmos.*, *120*, 4352–4369, doi:10.1002/2014JD022394.

Tselioudis, G., B. R. Lipat, D. Konsta, K. M. Grise, and L. M. Polvani (2016), Midlatitude cloud shifts, their primary link to the Hadley cell, and their diverse radiative effects, *Geophys. Res. Lett.*, *43*, 4594–4601, doi:10.1002/2016GL068242.

Westerman, P., and B. K. Ahring (1987), Dynamic of methane production, sulfate reduction and denitrification in a permanently waterlogged alder swamp, *Appl. Environ. Microbiol.*, *53*, 2554–2559.

Wolff, E., and R. Spahni (2007), Methane and nitrous oxide in the ice core record, *Philos. Trans. R. Soc. London, Ser. A.*, *365*, 1775–1792.

Worden, J., et al. (2013), El Niño, the 2006 Indonesian peat fires, and the distribution of atmospheric methane, *Geophys. Res. Lett.*, *40*, 4938–4943, doi:10.1002/grl.50937.

Zazzeri, G., et al. (2016), Carbon isotopic signature of coal-derived methane emissions to atmosphere: From coalification to alteration, *Atmos. Chem. Phys. Discuss.*, doi:10.5194/acp-2016-235.